INSTITUTE OF PHYSICS PUBLISHING JOURNAL OF PHYSICS B: ATOMIC, MOLECULAR AND OPTICAL PHYSICS

J. Phys. B: At. Mol. Opt. Phys. **36** (2003) 3889–3897 PII: S0953-4075(03)62238-8

Alignment following Au L_3 photoionization by synchrotron radiation

H Yamaoka[1], M Oura[1], K Takahiro[2], T Morikawa[2], S Ito[3], M Mizumaki[4], S Semenov[5], N Cherepkov[5], N Kabachnik[6,7] and T Mukoyama[8]

[1] Harima Institute, RIKEN (The Institute of Physical and Chemical Research), 1-1-1 Kouto, Mikazuki, Sayo, Hyogo 679-5148, Japan
[2] Kyoto Institute of Technology, Matsugasaki, Sakyo, Kyoto 606-8585, Japan
[3] Atomic Energy Research Institute, Kinki University, 3-2-1 Kowakae, Higashi-Osaka 577-8502, Japan
[4] Japan Synchrotron Radiation Research Institute (JASRI), 1-1-1 Kouto, Mikazuki, Sayo, Hyogo 679-5198, Japan
[5] State University of Aerospace Instrumentation, 190000 St Petersburg, Russia
[6] Fritz-Haber-Institut der MPG, Faradayweg 4-6, D-14195 Berlin, Germany
[7] Institute of Nuclear Physics, Moscow State University, Moscow 119992, Russia
[8] Kansai Gaidai University, 16-1 Nakamiya-Higashinocho, Hirakata, Osaka 573-1001, Japan

Received 15 April 2003, in final form 16 July 2003
Published 12 September 2003
Online at stacks.iop.org/JPhysB/36/3889

Abstract

The alignment of Au^+ ions following L_3 photoionization has been studied using a high-resolution x-ray spectrometer. We observed a small anisotropy for the angular dependence of Au L_ι and Lα emissions. The alignment parameter $\mathcal{A}_{20}$ derived from the experimental results is compared with theoretical calculations by Hartree–Fock approximation and random phase approximation with exchange. The contribution to the alignment of quadrupole interaction is discussed.

1. Introduction

Ionization of atoms leads to the 'alignment' of the inner-shell vacancy with the total angular momentum $J > 1/2$, where the magnetic sublevels of the resulting ion have a non-statistical population. The alignment effect can be measured from the non-isotropic angular distribution of the emitted Auger electrons and x-rays or from the polarization of the emitted photons. The alignment was predicted theoretically by Mehlhorn, Flügge *et al* and Jacobs [1–3]. In photoionization the alignment was first observed in Cd by Caldwell and Zare [4]. Recent photoionization experiments have used synchrotron radiation for measurements of the alignment [5–19]. Most of the experimental results were basically in agreement with the theoretical calculations [20–23].

On the other hand, the experimental results for the angular distributions of L x-rays from heavy elements were contradictory (see [24] and references therein). Recently we measured the angular dependence of Au and Pb L x-ray emissions following photoionization at the

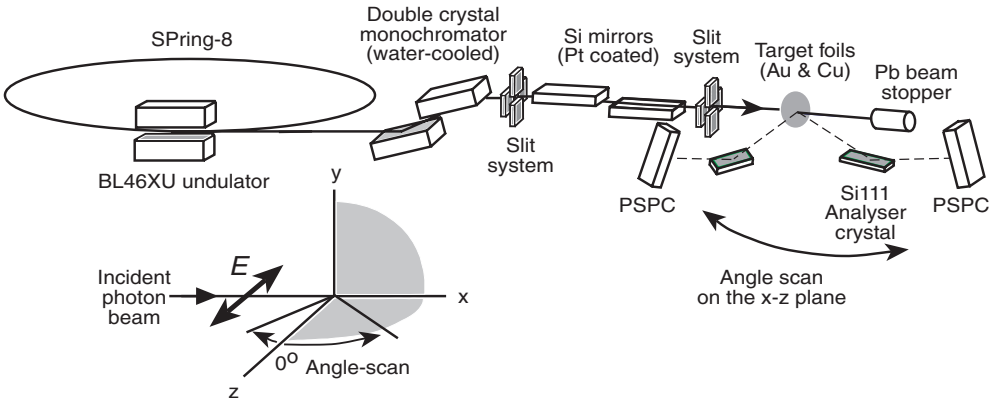

Figure 1. Schematic diagram of the experimental set-up. The energy dispersion plane of the analyser crystal is vertical with respect to the ground. The angle scan was performed in the photon beam transmitted side of the sample. The coordinate system used for the analyses is also shown.

SPring-8 facility. The results showed no evidence of L x-ray anisotropy (within experimental errors) for all incident photon energies, but in the case of L_ι x-rays an anisotropy of a few per cent might be possible [24]. These experimental results were in agreement with the Hartree–Fock (HF) theoretical calculations. However, all the previous experiments for photoionized L x-rays in heavy elements, including ours, had two disadvantages. One is relatively low energy resolution, so that we could not resolve lines such as $L\alpha_1$ and $L\alpha_2$. The other is the presence of the low-energy tail (the response function effect) that is inherent to the use of the Si(Li) solid-state detector (SSD) and this effect causes larger uncertainty in the estimation of the low-intensity signal. For example, the curve fit of the L_ι line, which is expected to have the largest anisotropy, was not easy because it is located on the large low-energy tail of the strong $L\alpha$ line. Furthermore, as the atomic number increases, the alignment effect becomes smaller. To determine the value of the anisotropy parameters more exactly for high-Z elements such as Au, it is indispensable to measure the emission lines with higher energy resolution.

In this paper we present the first high-resolution measurement of the angular dependence of L x-ray emissions from Au following photoionization by synchrotron undulator radiation at SPring-8. The experimental results are compared with the theoretical calculations made using the HF approximation and the random phase approximation with exchange (RPAE). The largest anisotropy is expected when the excitation energy is tuned between the L_2 and L_3 subshell ionization thresholds, because here only the L_3 subshell is ionized and there is no dilution effect due to the Coster–Kronig transitions.

2. Experiment

In the present experiment we utilized a crystal spectrometer instead of the Si(Li) SSD to avoid the difficulties described above for the Au target. Figure 1 shows a schematic diagram of the experimental set-up. The experiment was carried out at the undulator beamline BL46XU of SPring-8.[9]

A monochromatic photon beam ($E/\delta E \sim 10\,000$ at 8 keV, where E is the energy) was obtained using a double crystal monochromator cooled by water. The incident photon flux is

[9] See, for example, http://www.spring8.or.jp/e/facility/bl/SPring8BL/BL46XU/index.html.

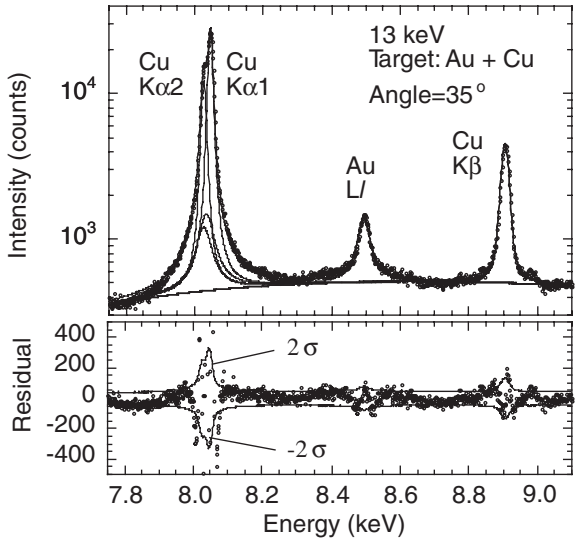

Figure 2. Upper panel: an example of the measured spectrum (filled circles) and fitted curves (solid curves) at the incident photon energy of 13 keV for a detector angle of 35°. The convoluted curve (solid curve) of each fitted curve, which coincides with the data points, is also shown. Lower panel: the residuals between the experimental data and the fitted curve. The solid curves denote the $\pm 2\sigma$ values of the data, where σ is the standard deviation.

of the order of 10^{12}–10^{13} photons s^{-1} at the target position. The target and the spectrometer were set on a Huber 5020 eight-axis diffractometer. The sample thickness (0.25 μm) was chosen to reduce the self-absorption effect. Intense synchrotron radiation could compensate the reduction of the emission signal due to the thin foil target. The incident photon beam was linearly polarized ($P_{\rm lin} \geqslant 99\%$) with the electric vector in the horizontal direction. A Si(111) flat crystal (about 10 cm long) with a position sensitive proportional counter (PSPC) was used as an analyser. We used the PSPC central area of about 50–60% so that we could ignore its edge effect.

The spectrometer was angle-scanned in the horizontal plane. The energy dispersion plane of the analyser crystal is vertical with respect to the ground. The energy resolution ($E/\delta E$) was about 250 at 9.713 keV. Before the target, we set two mirrors coated with Pt to reject the higher harmonics from the beamline monochromator. The incident energy was calibrated from the absorption spectrum of 50 μm-thick Pb L_3 edge (13.0352 keV) within an accuracy of ± 0.5 eV. The incident energy was tuned to be 13.002 keV, which is between the L_2 (13.7336 keV) and L_3 (11.9187 keV) edges and far from the Pt L-absorption edges. The scanning angle was measured with respect to the direction of the electric vector of the incident photon beam (see figure 1). The angular scan was performed in the photon beam transmitted side of the sample.

We could set the sample on the goniometer head within an accuracy of $\pm 1°$–$2°$. But the exact sample angle with respect to the incident photon beam was corrected by setting an ionization chamber just after the target and by measuring the change in the incident photon intensity while the sample angle was changed. In this measurement the angle that gave the maximum intensity was the one normal to the incident beam direction.

The angular distribution of L x-rays was measured at every 5° in the detector angle range from $-15°$ to 55°. The 10 h angle-scan was repeated 2–4 times under the same condition, and the results of each scan were summed up at each angle when we analysed the data.

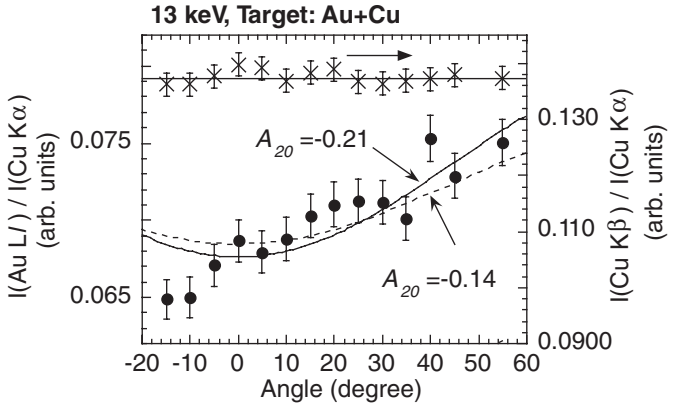

Figure 3. The angular distributions of Au L_ι (solid circles) and Cu Kβ (crosses) x-rays normalized to the Cu Kα x-ray intensity. Cu foil was attached to the Au target. The result of the curve fit (solid line) is also shown. The dashed curve shows a theoretical curve fit.

3. Results and discussion

In figure 2, the upper panel shows an example of the measured spectrum (filled circles) and fitted curves (solid curves) at the incident photon energy of 13 keV for the detector angle of 35°. The convoluted curve (solid curve) of each fitted curve, which coincides with the data points, is also shown. The lower panel in figure 2 shows the residuals between the experimental data and the fitted curve. The spectra were analysed by using the least-square fitting method with a Voigt function for each peak and a polynomial function for the background. The spectrum of Cu Kα was fitted by four Voigt functions, as performed by Deutsch *et al* [25]. The spectra obtained here were very similar; we could apply the same fitting procedure for all the spectra and thus the relative error of the line intensity for the change in the detector angle became small. The analysis was much simpler than for the experiments using the Si(Li) SSD because there was no low-energy tail for each line. The statistical error was less than 1% and the error of the fitting procedure was estimated to be about 1% for the Au L_ι line. The total error was, for example, about 2% for the Au L_ι line.

The line intensities were corrected for the effects of the incident beam attenuation, self-absorption of the emitted x-rays, absorption by air between the sample and the detector, the calculated Si(111) crystal reflectivity, and the PSPC efficiency. The relative difference in self-absorption correction for the change in detector angle was less than about 1% because we used thin foils. Since the attenuation of the emitted photons was caused mainly by the air between the sample and the detector, this effect was the same for any scanned angle. The PSPC detection efficiency with Pr gas (Ar mixed with 10% CH_4, 3 atm) changed from about 36% at 8.03 keV (Cu Kα_2) to about 25% at 9.71 keV (Au Lα_1). The calculated crystal reflectivity showed a change of about 14% when the energy was changed from 8.03 to 9.71 keV. However, when we compared the relative change in each line intensity as a function of the detector angle, the most effective correction terms were due to the incident beam attenuation and self-absorption. However, their effect was small, as described above.

Figure 3 shows the experimental angular distributions at 13 keV incident photon energy. In this measurement a Cu foil (0.5 μm thick) was attached to the Au foil to use the Cu K lines for the incident beam intensity monitor, and also to confirm the angular independence of the Cu K x-rays. As shown in figure 2, the Cu Kα lines have the satellite lines due to

the two- or three-hole transitions, except 1s–2p transitions [25]. When there are additional vacancies, the angular distribution of x-ray emission may be influenced [26–30]. But, as seen clearly in figure 3, in our experiment the intensity ratio of the Cu Kβ to Cu Kα x-rays is almost constant. Thus we used Cu Kα lines to normalize the intensity of the Au L_ι line. It is clear that the normalized intensity of the Au L_ι line has apparent angular dependence. In the previous experiments using the Si(Li) SSD the error was about $\pm$5–6% [24], while in this experiment it is less than $\pm$2% with better signal-to-noise ratio because of the high-energy resolution. It is noted that, when the multiple vacancies in Au are produced through the shake-up and shake-off processes for M and N shells, the probability is estimated to be less than 2×10^{-3} for M shells (summed up over all M shells) and less than 8×10^{-3} for N shells by using Dirac–Fock–Slater wavefunctions. These results indicate that the effect of multiple ionization processes, i.e. the satellite effect, on the alignment is negligibly small.

Theoretically, the angular distribution of the fluorescence radiation emitted after ionization of an atom by linearly polarized photons is described by the standard equation [31, 32], valid in the dipole approximation:

$$\frac{\mathrm{d}I}{\mathrm{d}\Omega} = \frac{I_0}{4\pi}[1 + \beta P_2(\cos\theta)], \tag{1}$$

where $P_2(\cos\theta)$ is the second Legendre polynomial, θ is the angle between the electric field vector of the exciting radiation and the direction of propagation of the fluorescence radiation, I_0 is the total fluorescence intensity integrated over all angles, and Ω is the solid angle. The anisotropy parameter β is a product of the kinematic term α_2^γ and the alignment parameter $\mathcal{A}_{20}$ of the initial state populated in the photoionization by linearly polarized light [20, 31]:

$$\beta = \alpha_2^\gamma \mathcal{A}_{20}(J_1), \tag{2}$$

where α_2^γ is calculated according to

$$\alpha_2^\gamma = \sqrt{\tfrac{3}{2}(2J_1+1)}(-1)^{J_1+J_2+1} \begin{Bmatrix} 1 & J_1 & J_2 \\ J_1 & 1 & 2 \end{Bmatrix}. \tag{3}$$

The values of α_2^γ calculated in [32] are $1/2$, $-2/5$, and $1/10$ for the emissions of L_ι (L_3M_1), Lα_2 (L_3M_4), and Lα_1 (L_3M_5) x-rays, respectively. The K vacancy ($J_1 = 1/2$) cannot be aligned and, correspondingly, the α_2^γ parameter is zero for all K x-rays. This indicates that, theoretically, the ratio of the Kβ to the Kα x-rays should not depend on the emission angle.

In the experiment we used the analyser crystal, which was polarization sensitive, to measure the x-ray emissions. In this case, under the conditions of our experiment, we need to use the following formula in the analysis [30, 33]:

$$\frac{\mathrm{d}I}{\mathrm{d}\Omega} = \frac{I_0}{8\pi}\left[1 + \beta\left(P_2(\cos\theta) - Q\frac{3}{2}\sin^2\theta\right)\right], \tag{4}$$

where Q is the polarization sensitivity, which is written as

$$Q = \frac{1 - |\cos 2\psi|^n}{1 + |\cos 2\psi|^n}, \qquad (1 \leqslant n \leqslant 2), \tag{5}$$

where ψ is the Bragg angle of the spectrometer crystal. For the perfect crystal the value of n is 1; for the ideal mosaic crystal the figure $n = 2$ is used. In the experiment we used a perfect Si crystal with Si(111) reflection ($2d = 0.6271$ nm, where d is lattice spacing) and $n = 1$ for the analysis. The values of Q are then estimated to be 0.043, 0.044 and 0.057 for Lα_1, Lα_2 and L_ι, respectively.

In figure 3 the dashed curve is the theoretical curve calculated using equation (4) with the alignment parameter $\mathcal{A}_{20} = -0.14$ obtained from the non-relativistic HF approach [24, 34, 35]; the solid curve shows the fitted curve to the experimental data. The experimental value for the

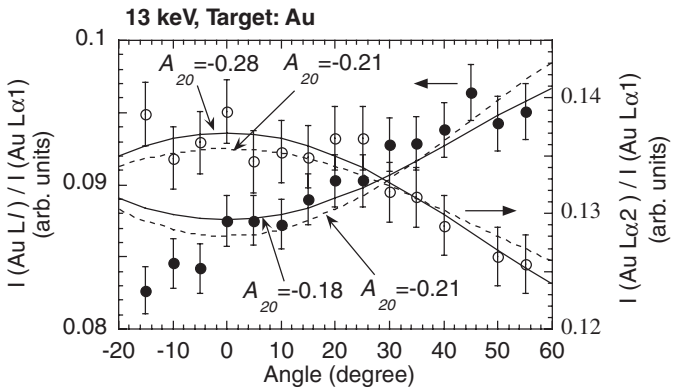

Figure 4. Angular distributions of Au L_ι (solid circles) and $L\alpha_2$ (open circles) x-rays normalized to the Au $L\alpha_1$ line intensity at incident photon energies of 13 keV. The solid curves show the results of the curve fits. The dashed curves are curves for $\mathcal{A}_{20} = -0.21$.

alignment parameter obtained from the curve fit for the L_ι line intensity is $\mathcal{A}_{20} = -0.21 \pm 0.04$, which is larger in magnitude than the theoretical prediction. It is interesting that, in a recent experiment by Küst *et al* [36] for the L_3 alignment in Xe, the experimental values are lower than those predicted by the same theory. One of the possibilities for explaining this discrepancy might be the narrow angular range of the present experiment. In our measurement the measured angular range is narrower compared to that of Küst *et al* [36] and does not include the data near the local maximum or minimum, although the number of the data points is much larger. This narrow angular range may lead to a larger systematic error when we determine the value of $\mathcal{A}_{20}$ through the curve-fitting procedure. The other possibilities from the theoretical side will be discussed later.

Figure 4 shows the angular dependence for the L_ι and $L\alpha_2$ lines normalized to the $L\alpha_1$ line intensity. In this measurement the target was Au only and we measured Au $L\alpha$ and L_ι lines by changing the analyser crystal Bragg angle. The angular dependence of the $L\alpha_1$ x-rays will be small, because the value of α for $L\alpha_1$ is $1/10$ but those for L_ι and $L\alpha_2$ are $1/2$ and $-2/5$, respectively. Theoretically, the normalized ratios of the L_ι and $L\alpha_2$ intensities to the $L\alpha_1$ intensity should have opposite behaviour when we observe the angular dependence, because the sign of the β is opposite. This tendency is clearly demonstrated in figure 4. The solid curves show the results of the curve fits. We can derive the alignment parameter through the curve fit, because the parameter is the same for all lines of $L\alpha$ and L_ι. As shown in figure 4, the value of the alignment parameter derived from the fit for L_ι is close to that presented above for the Au/Cu measurement, although the parameter derived from the fit for $L\alpha_2$ is slightly larger.

On the other hand, the theoretical values cited above were calculated in a simple independent-particle model, disregarding electron–electron correlations. Besides, the dipole approximation was used for the photon–atom interaction, although the photon energy is rather high (about 13 keV). To test these approximations, we have calculated the alignment of photo-ions within the RPAE including quadrupole interaction. If both dipole and quadrupole photon–atom interactions are considered, the angular distribution of subsequent fluorescence is modified to [27, 37]

$$\frac{\mathrm{d}I}{\mathrm{d}\Omega} = \frac{I_0}{4\pi}\left\{1 + \alpha_2^\gamma\left[\mathcal{A}_{20}P_2(\cos\theta) + \sqrt{\frac{3}{2}}\mathcal{A}_{22}\sin^2\theta\cos 2\phi\right]\right\}. \tag{6}$$

$\mathcal{A}_{22}$ is the $\kappa = 2$ component of the second-rank normalized statistical tensor $\mathcal{A}_{2\kappa} = \rho_{2\kappa}/\rho_{00}$, which describes anisotropy of the intermediate ionic state (we remember that the z-axis is chosen along the linear polarization vector and, in our geometry, $\phi = 0$). We note here that the non-dipole terms contribute to the alignment parameter $\mathcal{A}_{20}$ and determine entirely the third term in (6), proportional to $\mathcal{A}_{22}$. The general expression for the statistical tensors of photo-ions, including non-dipole corrections [37], can be reduced to the following form:

$$\rho_{k\kappa}(j_0, j_0) = (-1)^{j_0+l_0+1/2}(2j_0+1)\begin{Bmatrix} j_0 & l_0 & 1/2 \\ l_0 & j_0 & k \end{Bmatrix}\left(\sum_l \tfrac{1}{3}\begin{Bmatrix} l_0 & 1 & l \\ 1 & l_0 & k \end{Bmatrix}|d_l|^2\rho^{\gamma}_{k\kappa}(1,1) + \sum_l \tfrac{1}{5}\begin{Bmatrix} l_0 & 2 & l \\ 2 & l_0 & k \end{Bmatrix}(\alpha\omega)^2|q_l|^2\rho^{\gamma}_{k\kappa}(2,2)\right). \tag{7}$$

Here j_0 and l_0 are the total and orbital angular momenta of the vacancy produced in photoionization, l is the orbital angular momentum of the emitted electron, $\rho^{\gamma}_{k\kappa}(1,1)$ and $\rho^{\gamma}_{k\kappa}(2,2)$ are the dipole and quadrupole photon statistical tensors, respectively (see [37]), d_l and q_l are the dipole and quadrupole single-particle matrix elements as defined by Cherepkov and Semenov [38, 39], α is a fine-structure constant, and ω is a photon frequency. Expression (7) is obtained for a closed-shell atom.

Since the interaction of the valence electrons with a deep inner shell in heavy atoms is very weak, we ignore it and apply (7) to our case of the Au atom. The dipole and quadrupole amplitudes have been calculated within the non-relativistic RPAE [40]. If the quadrupole amplitudes are disregarded (dipole approximation), the resulting alignment for the photon energy of 13 keV is $\mathcal{A}_{20} = -0.120$, which is slightly less in magnitude than in the HF calculations. If the quadrupole amplitudes are included, the ion anisotropy is no longer characterized by one parameter, i.e. $\mathcal{A}_{20}$ (see equation (6)). However, in the geometry of our experiment, the angular distribution can still be presented in the form $1+\beta P_2(\cos\theta)$ with some effective alignment parameter. The calculations show that this parameter is $\mathcal{A}^{\mathrm{eff}}_{20} = -0.122$, i.e. the non-dipole contribution is indeed very small (<2%), as was predicted earlier [37].

Concluding this short theoretical analysis, we also give the value derived from early calculations by Scofield [27], who took into account the non-dipole corrections but calculated the single-electron wavefunctions within a simplified Hartree–Slater approach. The alignment value is $\mathcal{A}^{\mathrm{eff}}_{20} = -0.150$. One sees that all discussed models give very similar results, which are smaller in magnitude than obtained in our experiment. As a whole, the tendency of the experimental curve in figure 3 shows agreement with the theoretical predictions for the change in the L_ι line intensity, although there is still a discrepancy for the value of $\mathcal{A}_{20}$. Here we performed non-relativistic calculations. A fully relativistic calculation had been performed only by Johnson and Chen [22], but that was for the lighter atoms of Xe. The relativistic effect could be one of the main reasons for the above discrepancy, and the relativistic calculations for heavier atoms such as Au would be desirable.

4. Conclusion

The alignment of Au^+ ions following L_3 photoionization has been studied using a high-resolution x-ray spectrometer on synchrotron undulator radiation at the SPring-8 facility. The largest anisotropy is expected when the excitation energy is tuned between the L_2 and L_3 subshell ionization thresholds of Au. We observed a small anisotropy for the angular dependence of Au L_ι and $L\alpha_2$ emissions. Although the behaviour of the angle dependence agrees with the theoretical predictions, the alignment parameter $\mathcal{A}_{20}$ derived from the experimental results is slightly larger than that obtained from the theoretical calculations

within the HF approximation and RPAE. The contribution of quadrupole interaction to the alignment is calculated and the effect is small. A reason for the discrepancy between theory and experiment is probably the fact that the alignment was calculated with non-relativistic wavefunctions. Full relativistic calculations are therefore necessary. In the experiment it is preferable that the measured data points include the maximum and/or minimum intensity region for better curve fitting in order to obtain a more exact value of the alignment parameter. It is also interesting to see the energy dependence of the alignment parameter and the Coster–Kronig transition effect on the alignment by changing the incident photon energy between the L edges. These experiments will be undertaken in the future.

Acknowledgments

We are grateful to Dr S Goto for his calculation of the reflectivity in the crystal, and to Professor K Kawatsura for encouragement. We also thank Professor W Mehlhorn and Dr U Kleiman for useful information about their recent results of experiments and calculations. The experiments were performed at the SPring-8 facility of the Japan Synchrotron Radiation Research Institute (JASRI) under Proposal No 2002B0089-CS2-np. NK is grateful to the Fritz-Haber-Institut der MPG for hospitality and financial support.

References

[1] Mehlhorn W 1968 *Phys. Lett.* A **26** 166
[2] Flügge S, Mehlhorn W and Schmidt V 1972 *Phys. Rev. Lett.* **29** 7
[3] Jacobs V L 1972 *J. Phys. B: At. Mol. Phys.* **5** 2257
[4] Caldwell C D and Zare R N 1977 *Phys. Rev.* A **16** 255
[5] Southworth S H, Kobrin P H, Truesdale C M, Lindle D, Owaki S and Shirley D A 1981 *Phys. Rev.* A **24** 2257
[6] Southworth S, Becker U, Truesdale C M, Kobrin P H, Lindle D W, Owaki S and Shirley D A 1983 *Phys. Rev.* A **28** 261
[7] Kronast W, Huster R and Mehlhorn W 1984 *J. Phys. B: At. Mol. Phys.* **17** L51
[8] Kronast W, Huster R and Mehlhorn W 1986 *Z. Phys.* D **2** 285
[9] Kämmerling B, Hausmann A, Lüger J and Schmidt V 1992 *J. Phys. B: At. Mol. Opt. Phys.* **25** 4773
[10] Kämmerling B, Krässig B, Schwarzkopf O, Ribeiro J P and Schmidt V 1992 *J. Phys. B: At. Mol. Opt. Phys.* **25** L5
[11] Whitfield S B, Caldwell C D, Huang D X and Krause M O 1992 *J. Phys. B: At. Mol. Opt. Phys.* **25** 4755
[12] Schmoranzer H, Lauer S, Vollweiler F, Ehresmann A, Sukhorukov V L, Lagutin B M, Petrov I D, Demekhin Ph V, Schartner K-H, Magel B and Mentzel G 1997 *J. Phys. B: At. Mol. Opt. Phys.* **30** 4463
[13] Mentzel G, Schartner K-H, Wilhelmi O, Magel B, Staude U, Vollweiler F, Lauer S, Leibel H, Schmoranzer H, Sukhorukov V L and Lagutin B M 1998 *J. Phys. B: At. Mol. Opt. Phys.* **31** 227
[14] Snell G, Kukk E, Langer B and Berrah N 2000 *Phys. Rev.* A **61** 042709
[15] Yenen O, McLaughlin K W, Jaecks D H, Sant'Anna M M and Seddon E A 2001 *Phys. Rev. Lett.* **86** 979
[16] Meyer M, Marquette A, Grum-Grzhimailo A N, Kleiman U and Lohmann B 2001 *Phys. Rev.* A **64** 022703
[17] McLaughlin K W, Yenen O, Jaecks D H, Gay T J, Sant'Anna M M, Calabrese D and Thaden-Jordan B 2002 *Phys. Rev. Lett.* **88** 123003
[18] O'Keeffe P O, Alise S, Meyer M and Grum-Grzhimailo A N 2003 *Phys. Rev. Lett.* **90** 023002
[19] Lagutin B M, Petrov I D, Sukhorukov V L, Kammer S, Mickat S, Schill R, Schartner K-H, Ehresmann A, Shutov Yu A and Schmoranzer H 2003 *Phys. Rev. Lett.* **90** 073001
[20] Berezhko E G, Kabachnik N M and Rostovsky V S 1978 *J. Phys. B: At. Mol. Phys.* **11** 1749
[21] Bartschat K 1987 *J. Phys. B: At. Mol. Phys.* **20** 5023
[22] Johnson W R and Chen K T 1992 *Phys. Rev.* A **46** 2952
[23] Kleiman U and Lohmann B 2003 *J. Electron Spectrosc. Relat. Phenom.* at press
[24] Yamaoka H, Oura M, Takahiro K, Takeshima N, Kawatsura K, Mizumaki M, Kleiman U, Kabachnik N and Mukoyama T 2002 *Phys. Rev.* A **65** 062713
[25] Deutsch M, Hölzer G, Härtwig J, Wolf J, Fritsch M and Förster E 1995 *Phys. Rev.* A **51** 283
[26] Pedersen E H, Czuchlewski S J, Brown M D and Ellsworth M D 1975 *Phys. Rev.* A **11** 1267

[27] Scofield J H 1976 *Phys. Rev.* A **14** 1418
[28] Jitschin 1984 *J. Phys. B: At. Mol. Phys.* **17** 4179
[29] Papp T and Kocbach L 1987 *J. Physique* C **9** 243
[30] Papp T 1999 *Nucl. Instrum. Methods* B **154** 300
[31] Balashov V V, Grum-Grzhimailo A N and Kabachnik N M 2000 *Polarization and Correlation Phenomena in Atomic Collisions: a Practical Theory Course* (New York: Kluwer) p 159
[32] Berezhko E G and Kabachnik N M 1977 *J. Phys. B: At. Mol. Phys.* **10** 2467
[33] Cleff B 1982 *Acta Phys. Pol.* A **61** 285
[34] Kleiman U and Lohmann B 2000 *J. Phys. B: At. Mol. Opt. Phys.* **33** L641
[35] Kleiman U 2002 *J. Phys. B: At. Mol. Opt. Phys.* **35** 947
[36] Küst H, Kleiman U and Mehlhorn W 2003 *J. Phys. B: At. Mol. Opt. Phys.* **36** 2073
[37] Kabachnik N M and Sazhina I P 1996 *J. Phys. B: At. Mol. Opt. Phys.* **29** L515
[38] Cherepkov N A and Semenov S K 2001 *J. Phys. B: At. Mol. Opt. Phys.* **34** L211
[39] Cherepkov N A and Semenov S K 2001 *J. Phys. B: At. Mol. Opt. Phys.* **34** L495
[40] Amusia M Ya and Cherepkov N A 1975 *Case Stud. At. Phys.* **5** 47